

Amyloid β Peptides Aggregation in a Mixed Membrane Bilayer: A Molecular Dynamics Study

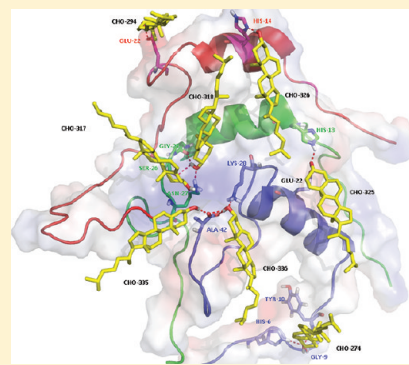
Li Na Zhao,[†] See-Wing Chiu,[‡] Jérôme Benoit,[†] Lock Yue Chew,^{*,†} and Yuguang Mu^{*,§}

[†]School of Physical and Mathematical Sciences, Nanyang Technological University, Singapore 637371

[‡]Beckman Institute, University of Illinois at Urbana-Champaign, Urbana, Illinois 61801, United States

[§]School of Biological Sciences, Nanyang Technological University, 60 Nanyang Drive, Singapore 637551

ABSTRACT: The aggregation of amyloid β peptides resulting in neurotoxic oligomers is an important but yet mysterious process in Alzheimer's disease development. Molecular dynamics simulations were performed to investigate the self-assembly of three full-length amyloid peptides in the zwitterionic dipalmitoylphosphatidylcholine and cholesterol mixed lipid bilayer. During the 1000 ns simulation, the residues 1–27 were found to interact preferentially with the lipid–aqueous interface region, while residues 28–42 show an inclination to remain inside the bilayer hydrophobic tail region. The interaction between peptides and lipids has facilitated the association of $A\beta$ peptides. However, the interaction between cholesterol and peptides is inversely correlated with the extent of the peptide–peptide interactions. Our simulation has uncovered the formation of a short segment of parallel β -sheet between two peptide chains. In another chain, the N- and C-termini came close to each other. All the structural transitions indicate that our simulation has caught a glimpse of the complicated peptide oligomerization process. The full understanding of the underlying mechanism still requires further experimental and theoretical studies.



INTRODUCTION

Alzheimer's Disease (AD) is characterized by the extra-neuronal Amyloid β ($A\beta$) plaque and intraneuronal fibrillar tangles. The Amyloid β plaques result from the aggregation of the Amyloid β peptides, which are cleaved by the β - and γ -secretase from Amyloid precursor protein (APP).^{1,2} Studies show that even before the $A\beta$ plaque forms the neuron has already been damaged, and further researches show that the $A\beta$ oligomers may be the candidate which causes the neurotoxicity.^{3–6} The oligomers usually have no regular or only transient secondary structures. They often attach to the membrane or other macromolecules and become insoluble.⁷ Thus, it is difficult for conventional experimental tools to study the toxicity mechanism. Complementary to the experimental methods, molecular dynamics simulation is a theoretical tool for atomic-detailed study of aggregation process and the influence of environmental factors such as pH, lipid membrane, etc.

There exist several hypotheses of the toxicity mechanism,⁸ one of which suggests that the binding of the excessive $A\beta$ peptides to the membrane receptors, such as glutamate receptor, has affected their functions.⁹ Another points to the formation of the membrane pore/channel,^{10–13} which leads to the alteration of the ionic homeostasis.^{14,15} To understand the mechanism of amyloid toxicity, $A\beta_{42}$ oligomers have been studied in an implicit membrane, and it was found that the identified β -sheet structure exhibits the typical strand–turn–strand motif.¹⁶ In a dipalmitoylphosphatidylcholine (DPPC) bilayer environment, the structure and the insertion depth of a single $A\beta_{40}$ peptide¹⁷ and the relevant conformational change of the membrane¹⁸ have been

studied. In another palmitoyleoleylphosphatidylglycerol (POPG) lipid bilayer environment, six preformed $A\beta_{25–35}$ β -sheets have been inserted into the POPG in different ways. A water-permeable pore is observed to result, which is accompanied by a strongly disturbed local membrane structure.¹⁹

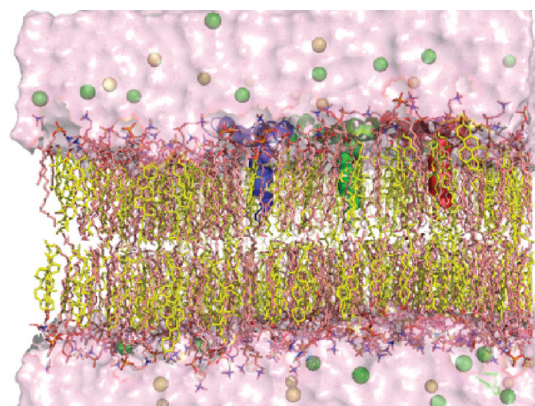
Replica exchange molecular dynamics simulation has been performed to study the short peptide $A\beta_{10–35}$ dimer and trimer formation.²⁰ A coarse-grained model has also been employed to study the structural diversity of the dimer in aqueous environment and the diversity of kinetic pathways in the fibrillization process.^{21–23} A discrete molecular dynamics study shows that the C-terminal region of $A\beta_{42}$ plays an important role in its aggregation process.²⁴ A Monte Carlo simulation has also been used to study the dimer formation of several mutated $A\beta_{42}$ peptides, revealing that the intramolecular antiparallel β -sheet structures are shared by different $A\beta$ variants.²⁵

Another replica exchange molecular dynamics simulation study of the $A\beta_{42}$ monomer on the surface of DPPC and dioleylphosphatidylserine (DOPS) bilayer indicates that the interactions between $A\beta$ and lipids do not promote structural ordering, and the conformational dynamics is possibly restricted because of the interaction between the protein and the lipid.²⁶ Another all-atomic study of very short peptides ($Gly-Ala$)₄ and ($Gly-Val$)₄ in the presence of a water/n-octane mixture indicates that the non-polar planar octane–water interface facilitates the aggregation by

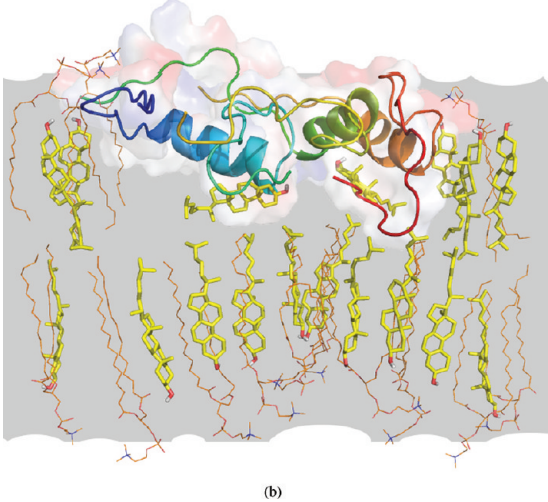
Received: July 12, 2011

Revised: September 9, 2011

Published: September 12, 2011



(a)



(b)

Figure 1. Simulation system. The three peptides are aligned in a parallel fashion in the cubic box as shown in the snapshot (peptide A, blue; peptide B, green; peptide C, red). The cholesterol are represented by yellow sticks and the DPPCs by orange lines. The green and yellow orange dots are Cl^- and Na^+ ions, respectively (a). A schematic representation of the defects of the membrane caused by protein perturbation. The three peptides are represented by cartoon and colored by spectrum. The cholesterol is shown as sticks and colored by elements (C, yellow; O, red; H, gray). The DPPC is represented by lines (b). The images are produced by PyMOL.

reducing the self-assembly dimension from three to two, thus increasing the concentration of oligomers.²⁷ A study of the $\text{A}\beta$ oligomers adsorption affinity toward the self-assembled monolayers by all-atom MD simulations has revealed the preferential adsorption of the C-terminal regions by monolayers, and the main driving force at the interface is the hydrophobic interaction.²⁸

Extensive experimental studies have also been carried out focusing on the aggregation and nucleation-elongation mechanism of fibril formation.^{29–31} $\text{A}\beta$ peptides are being produced in cholesterol-rich areas, and it is generally believed that there is a great risk of Alzheimer's disease in the presence of elevated cholesterol level.³² The relationship between $\text{A}\beta$ peptide binding to lipid and its aggregation in the membrane environment is not yet clear. A recent finding showed that the $\text{A}\beta$ peptides have the capacity of binding the microbial lipid bilayers as antimicrobial

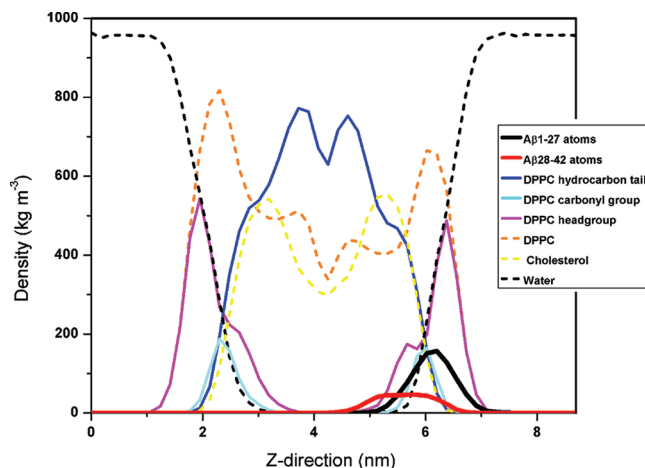


Figure 2. Partial density function along the Z-direction.

peptides except the incidental amyloidosis.³³ Another experimental study finds that $\text{A}\beta_{1-28}$ prefers to interact with the polar headgroup of lipids, while $\text{A}\beta_{25-40}$ tends to bury itself inside the hydrophobic core region of the membrane.³⁴ In experiments combining circular dichroism, thioflavin T fluorescence, size-exclusion chromatography, and transmission electron microscopy measurements, the $\text{A}\beta$ peptide was found to change its conformation from an α -helix-rich to a β -sheet-rich structure in a cholesterol-dependent manner.^{35,36}

It is important to get a detailed interacting picture of the association of the peptides with the lipid bilayers. Here we have conducted several simulations of the full-length $\text{A}\beta_{1-42}$ proteins in the membrane environment formed by mixed DPPC and cholesterol.

METHODS AND SIMULATION SETUP

The initial conformation of the full-length $\text{A}\beta_{1-42}$, whose sequence is DAEFRHDSGYEVHHQKLVFFAEDVGSNKGAIIGLMVGGVVIA, was taken from the model 1 of the Protein Data Bank (PDB) ID 1IYT.³⁷ The structure consists of two helical regions encompassing residues 8–25 and 28–38 which are connected by a regular type I β -turn. The protein was represented by the GROMOS96 43a1 force field. The membrane model was proposed by Chiu et al., which consists of cholesterol and DPPC (<http://www.nanoconductor.org/43A1-S3/>), and is represented by the 43A1-S3 parameter set.^{38–42} The DPPC and cholesterol mixed lipid bilayer were arranged to lie in the xy -plane and centered at the origin of the coordinate system. To speed up the simulation, the three $\text{A}\beta$ peptides were put in the vicinity of the pre-equilibrium mixed bilayer. Nine cholesterol and 31 DPPC molecules were found steric-clashing with the peptides and were removed from the upper leaflet. The final membrane composition is that there are 118 cholesterol and 96 DPPCs in the upper leaflet and 127 cholesterol and 127 DPPCs in the lower leaflet. The DPPC lipid was chosen because it has PC headgroups which are found to be abundant in neural membranes.⁴³ Three $\text{A}\beta$ proteins were solvated in the mixed bilayer and aligned parallel in a cubic box of dimensions $101.57 \text{ \AA} \times 105.03 \text{ \AA} \times 87.82 \text{ \AA}$. The center of masses of each of the proteins were placed at (35.79, 52.52, 65.82), (55.79, 52.52, 65.82), and (75.79, 52.52, 65.82) and were labeled as peptide A, B, and C, respectively. 14 947 water molecules with 65 Na^+ and 56 Cl^-

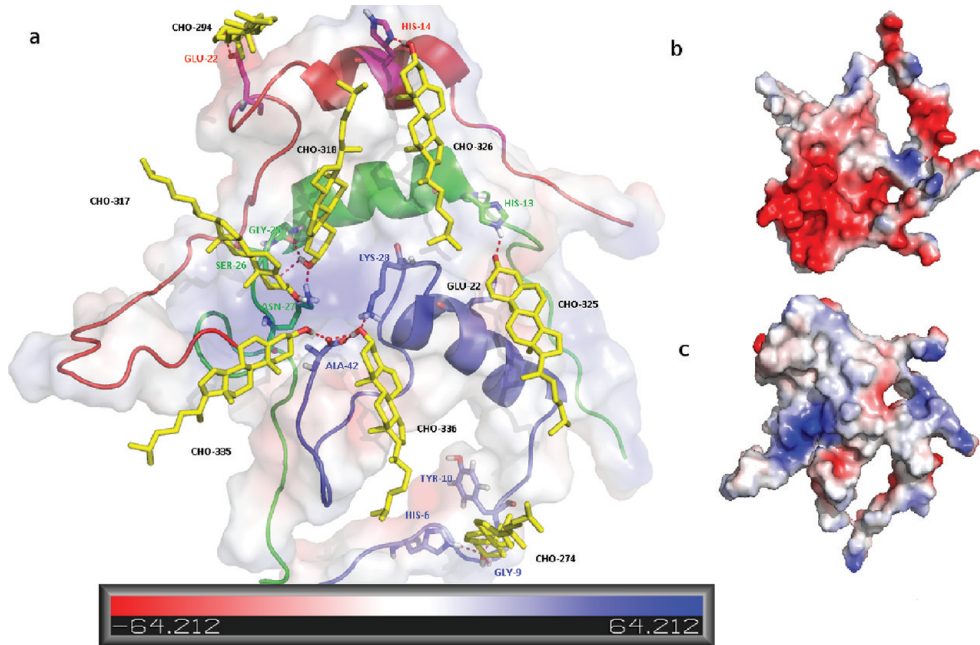


Figure 3. Snapshot of the binding of the cholesterol to the protein. The view is directed from the hydrophobic core toward the upper layer. The three peptides are represented in cartoon (peptide A, maroon; peptide B, green; peptide C, red). The cholesterol are shown as sticks and colored by element (C, yellow; H, gray; O, red). The residues TYR-10, GLU-22, LYS-28, and ALA-42 of peptide A are colored by element (C, maroon; N, blue; H, gray; O, red). HIS-13, GLY-25, SER-26, and ASN-27 of peptide B are colored by elements with green for carbon to distinguish it from the carbon of peptide A. The carbon atoms of HIS-14 and GLU-22 of peptide C are colored red to differentiate them from those of peptides A and B's residues, and they are all represented as sticks. The electrostatic surface potential of the protein is represented by the color scheme: red, negative; blue, positive; gray, neutral (a). The electrostatic potential surface of the protein with the view toward the membrane surface (b). The electrostatic potential surface of the protein viewed from the membrane surface (c).

ions were filled within the box to help neutralize and reach the concentration of 0.1 mol/L. The initial setup is shown in Figure 1(a).

All bonds were constrained using the linear constraint solver (LINCS)⁴⁴ algorithm with a 2 ps integration time step. The temperature was kept at 323 K using the Nosé–Hoover coupling scheme.^{45,46} It was chosen to be above the DPPC gel–liquid transition phase.⁴⁷ A semi-isotropic pressure coupling at 1 bar by means of a Parrinello–Rahman barostat with a coupling constant of 2 ps was used in the pressure ensemble. The van der Waals cutoff was set to 1.6 nm. The Particle Mesh Ewald method⁴⁸ was used for electrostatic interaction with a sixth-order interpolation and a Fourier grid spacing of 0.15 nm as recommended by the 43A1-S3 force field. Simulations of 1000 ns were conducted. The simulation and analysis were performed using facilities within the GROMACS package. PyMOL⁴⁹ and VMD⁵⁰ were used to visualize the structure.

RESULTS

Interaction between $\text{A}\beta_{42}$ and DPPC. Initially, residues 1–27 of the peptides were arranged on the surface of the membrane, and residues 28–42 were buried inside the membrane. The partial density profile of the water, DPPC headgroups and hydrocarbon tail, cholesterol, and residues 1–27 and 28–42 of $\text{A}\beta_{1–42}$ during the whole simulation time were plotted along the Z-direction (membrane normal direction). The DPPC carbonyl group atoms (CO) were also plotted to identify the boundary between the polar and hydrophobic regions (see Figure 2). From Figure 2, the interface between the DPPC hydrophilic head

Table 1. Order Parameter of the Hydrocarbon Tail of Cholesterol (From Carbon 22 to 25)

order parameter of cholesterol	
CHO-274	0.49
CHO-294	0.46
CHO-317	0.05
CHO-318	-0.18
CHO-325	0.29
CHO-326	-0.14
CHO-335	-0.14
CHO-336	-0.23

groups and the hydrophobic tails is clearly shown. The small dip around 4.4 nm is the region between the upper and lower monolayers. Due to the fact that the peptides were embedded initially in the upper leaflet, the density of DPPC and cholesterol in the upper leaflet is slightly lower than that of the lower leaflet. At the end of the simulation, the peptides have fully sunk inside the DPPC. Further scrutiny shows that residues 1–27 interact preferentially with the DPPC headgroup, while residues 28–42 prefer to remain inside the DPPC hydrophobic tail region. A recent experimental study by Ionov et al.³⁴ also showed the same tendency with $\text{A}\beta_{1–28}$ interacting with the hydrophilic headgroup and $\text{A}\beta_{25–40}$ locating in the hydrophobic tail region of the bilayer.

Interaction between $\text{A}\beta_{42}$ and Cholesterol. The binding of cholesterol onto the peptides has the effect of tilting the

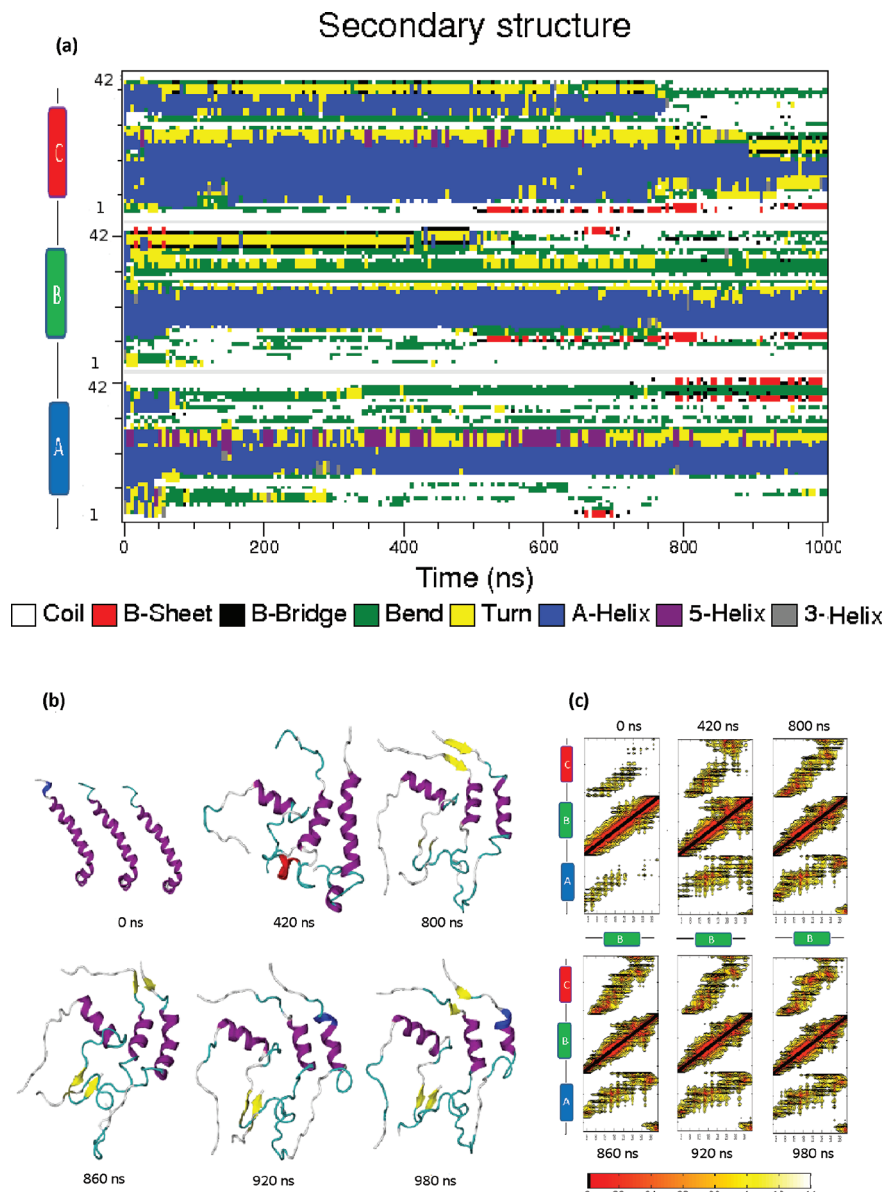


Figure 4. Conformational evolution of the $\text{A}\beta_{1-42}$ peptides in the mixed bilayer as a function of time. (a) The secondary structure is calculated by DSSP. (b) Snapshots of the secondary structures of peptides are colored based on their default representation in VMD (α -helix, purple; 3–10-helix, blue; π -helix, red; extended- β , yellow; bridge- β , tan; turn, cyan; coil, white). (c) The contact map of the residues of the three peptides. The contacts that form hydrogen bonding for peptides A and B and B and C are in dark red.

cholesterol from its original orientation which can be observed from Figure 3. The deuterium order parameter, which is usually used to describe the orientation of lipid chains,⁵¹ is used to quantify this tilt of the cholesterol. The equation of the deuterium order parameters S_{CD} is given as follows

$$S_{CD} = \frac{1}{2} (\langle 3 \cos^2 \theta \rangle - 1) \quad (1)$$

Here, θ is the angle between the C–D bond and the bilayer normal. S_{CD} can vary from -0.5 (parallel to the bilayer) to 1 (normal to the bilayer). Due to the rigidity of the cholesterol, only the order parameter for the top and the bottom carbon atoms of the hydrocarbon tail of the cholesterol (CHO) is calculated. From the order parameter in Table 1, we can see that CHO-318, CHO-326, CHO-335, and CHO-336 are

tilted to such a large extent as to be nearly perpendicular to the normal. The large tilt of the cholesterol at the side where $\text{A}\beta$ peptides are bound is caused by the presence of the peptides, but it could also be an artifact or at least be exaggerated by our initial modeling procedure. Nevertheless, for those cholesterols that are located far away from the peptides, they are found to possess higher values of the order parameter which implies that they are not tilted largely and still nearly perpendicular to the bilayer normal. We observed that the cholesterol has a greater tilt at the position where the electrostatic potential of the peptide surface is positive. The same positive potential surface also interacts extensively with the membrane lipids (see Figure 3c), while the potential of the interface between the peptides and water molecules is predominantly negative (see Figure 3b).

Structure of $\text{A}\beta_{42}$ Embedded in DPPC–CHOL Bilayers. The central step of the amyloidogenic oligomerization process is the transition from α -helix-rich to β -sheet-rich structures. The initial structure of the $\text{A}\beta$ peptide was determined by a 3D nuclear magnetic resonance (NMR) technique in the apolar microenvironment, namely, the hexafluoroisopropanol that mimics the lipid phase of the membrane, and it turned out to be α -helix predominantly.³⁷ During our 1 μs simulation, the α -helical structures at the N- and C-terminus of the $\text{A}\beta$ were observed to unfold, with the occasional formation of a 3–10-helix, before transforming into random coils and turns. At $t = 500$ ns, a short segment of the parallel β sheet was found to shape up between residues SER-8 and TYR-10 of chain B and residues GLU-3 and ARG-5 of chain C, and at around $t = 800$ ns, a β hairpin motif appeared at the C-terminus of chain A (see Figure 4). It is more likely that the α -helical structure unfolds at both termini, while the middle segment starting from HIS-14 to ASP-23 (namely, HQQLVFFAED) remains as an α -helix throughout the whole 1000 ns simulation, based on our DSSP⁵² analysis. Interestingly, from $t = 400$ ns onward, the N- and C-terminus of chain A were observed to come close to each other. Such conformation resembles the strand–loop–strand configuration in the structural model of protofibril.⁵³ It is clear that the time scale needed for the complete conversion from α -helix to β -sheet is far beyond 1000 ns. Nevertheless, our 1000 ns simulation has caught a glimpse of such a transition.

Peptide–Peptide Interactions in the Membrane. The three peptides were observed to form an invagination in the membrane bilayer (see Figure 1(b)). The perturbation of the peptides on the membrane has caused the nearby cholesterol molecules to tilt with a high degree. The void in the middle of the bilayer has induced the elongation of the DPPC chain and also the caving-in of the lower leaflet lipid molecules. The invagination is filled with protein and water. The invagination reaches a depth of 12 Å from the membrane surface at $t = 1000$ ns. From Figure 5, we can observe two deep wells in the P1 and P2 positions, where chain A and B and chain B and C make extensive hydrogen-bonding interactions with each other (see Figure 6). At the P1 site, the NH of the amide groups on the GLN-15 side chain and the imidazole group of HIS-14 from chain B both act as a hydrogen bond donor (2.2 Å and 2.0 Å) to the side chain and backbone carboxyl groups of ASP-7 of chain C, respectively. On the P2 site, residues ASN-27, along with the solvent-exposed residues GLU-22 and ASP-23, all from chain A, construct a hydrophilic “floor”, and they form hydrogen bonds with TYR-10 and LYS-16 of chain B. The favorable interaction between GLN-15 from chain A and the N-terminus of chain B also stabilizes the parallel β -sheet between chain B and chain C (see Figure 4(a) and 4(b) at snapshots $t = 800, 860$, and 980 ns), which might be important for the protofibril formation in the later stage.⁵⁴

The ALA-42 at the C-terminus of the two peptides, chain B and C, was found to play an important role in the formation of hydrogen bonds: the main chain amide and carbonyl group of ALA-42 from peptide B forms hydrogen bonds with the side chain carboxyl group and the main chain amide group of GLU-3 from peptide A; the carboxyl group of ALA-42 on the peptide C is tightly packed by a hydrogen bond network from the main chain amide groups of LYS-28, GLY-29, ALA-30, ILE-31, and ASN-27 of peptide B, of which ASN-27 is located near the end of the α -helix of peptide B (the ASN-27 of peptide A is also located near the end of the α -helix).

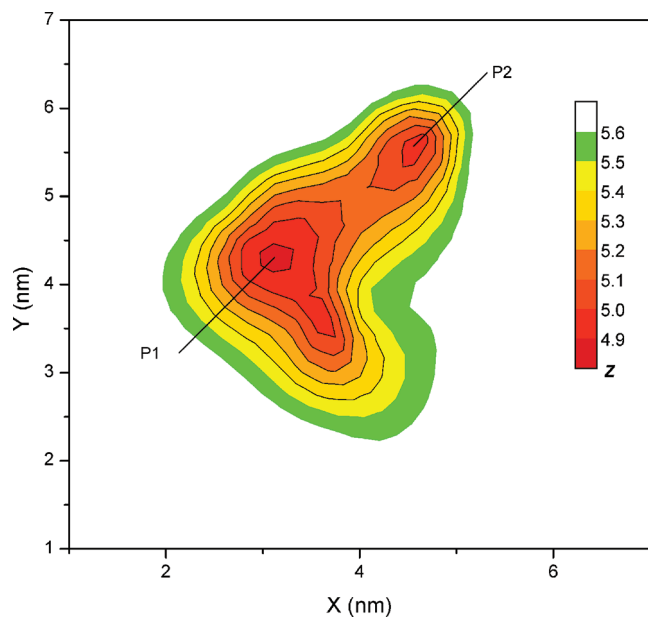


Figure 5. Contour map of the invagination. The depth z of the upper surface layer vs the position x , y as defined in the Methods and Simulation Setup section. Note that the white background is for surface depth $z > 5.6$ nm.

Interaction among Peptides, Cholesterol, and DPPC. The asymmetry of the initial arrangement of the peptides on the upper leaflet in our simulation system has made it necessary for us to examine the upper and lower leaflets separately. The order parameter profile (see Figure 7) of the DPPC sn-1 (aliphatic carbon atoms C15–C31 on the tail of DPPC) and sn-2 chains (aliphatic carbon atoms from 34 to 50 on the tail of DPPC) shows that the value of the order parameter of the lower leaflet is higher than that of the upper leaflet: on average the $\langle S_{CD} \rangle$ of the upper leaflet is 0.272 ± 0.047 lower than that of the lower leaflet, and the same holds for the cholesterol.

The radial distribution functions (RDFs) of the DPPC and cholesterol with respect to the peptides in the upper and lower leaflets were calculated (see Figure 8) with a distance binning of 0.2 Å. During the whole simulation, the peptides remain in the upper leaflet. The pairing of the peptides and cholesterol have a high possibility of locating at the distance of 5–15 Å in the upper leaflet, and the pairing between the peptides and DPPC lipids have a high propensity to locate at 4.5 ± 1.0 Å and 9.0 ± 1.0 Å. At a distance of 2.4 Å, small peaks are observed at the RDF profile indicating direct contacts (mainly through hydrogen bonds) between peptides and cholesterol and DPPC.

To further examine the relationship between the protein, DPPC, and cholesterol, we have calculated the RDFs between the hydroxyl oxygen atoms of cholesterol and the DPPC carbonyl oxygen atoms and the phosphate oxygen atoms for both the upper and lower leaflet. From Figure 9, one finds that the RDFs have a sharp peak around 2.5 Å for all four cases. The study of Chiu et al.⁵⁵ has shown that the lower the concentration of the cholesterol, the higher the peak of the RDF at 2.5 Å of the cholesterol oxygen with DPPC carbonyl oxygen. In our simulation, the number ratio of cholesterol to DPPC in the upper leaflet is 118:96, and in the lower leaflet, it is 127:127. We have also observed that the higher cholesterol concentration (in the upper leaflet) has led to a lower peak height than that in the lower

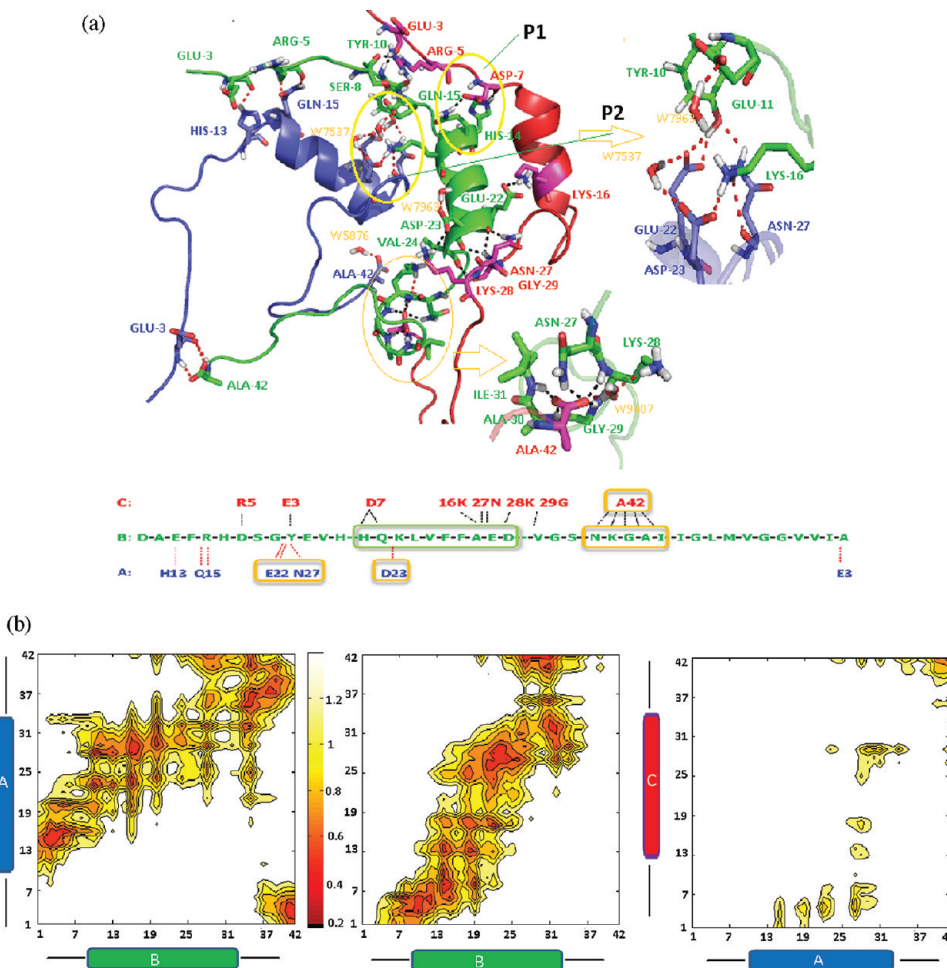


Figure 6. Details of the hydrogen bond configurations between peptide A and B and peptide B and C. Peptides A, B, and C are shown in cartoon and represented in blue, green, and red color, respectively. The hydrogen bonds between peptides A and B are indicated by red dash lines; the hydrogen bonds between peptides B and C are given by black dashed lines; and the hydrogen bonds between water and peptides are shown by red dash lines. The two yellow circles depict the P1 and P2 sites. The sequence below the figure gives a hydrogen bonding map between the three peptides (a). The contact map between the residues of three peptides. Note that the dark red region corresponds to residues connected by hydrogen bonds (b).

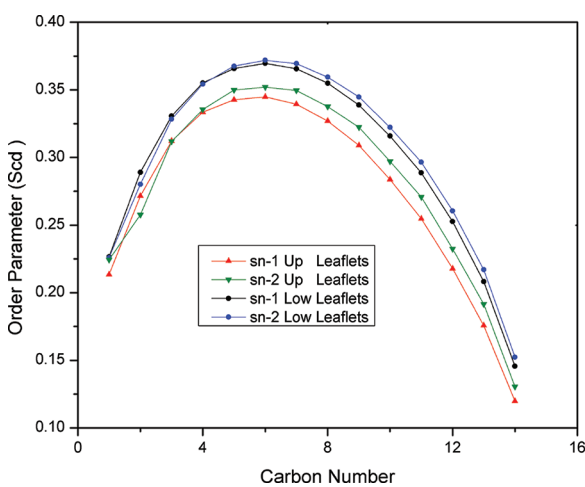


Figure 7. Order parameter profile for the DPPC sn-1 and sn-2 chains in the upper and lower leaflets.

leaflet. The sharp peak around 2.5 Å reflects the strong binding between the cholesterol and DPPC. The peptides present in the

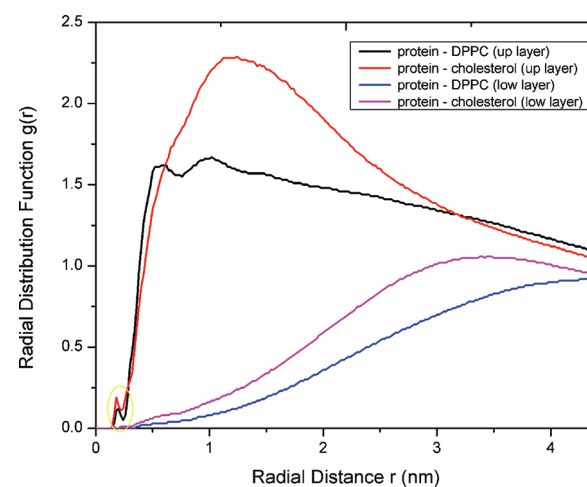


Figure 8. Plot of the RDFs of the DPPC and cholesterol with respect to the protein in the upper and lower leaflet.

upper leaflet compete with DPPC in the formation of hydrogen bonds with the cholesterol hydroxyl groups. This gives another

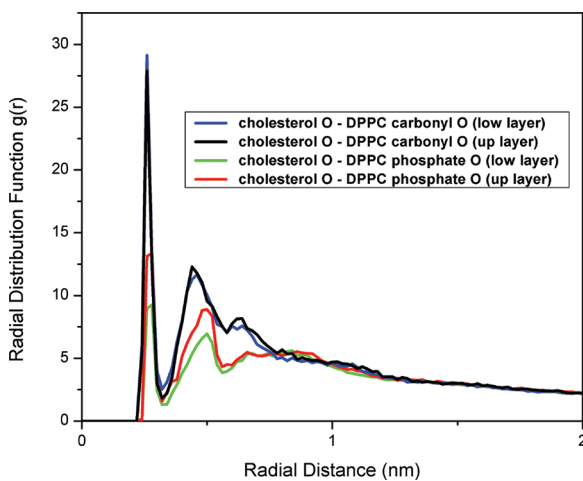


Figure 9. Plot of the RDFs between cholesterol O and DPPC phosphate and cholesterol O and DPPC carbonyl O, in the upper and lower leaflet.

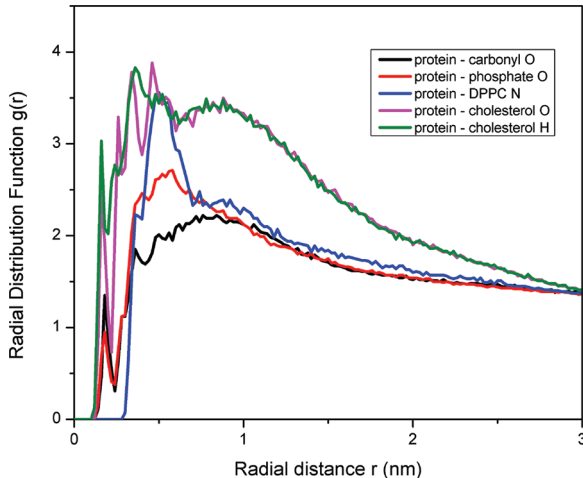
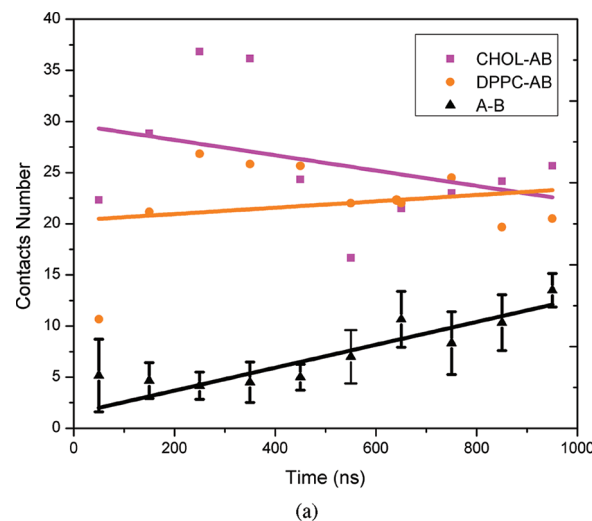


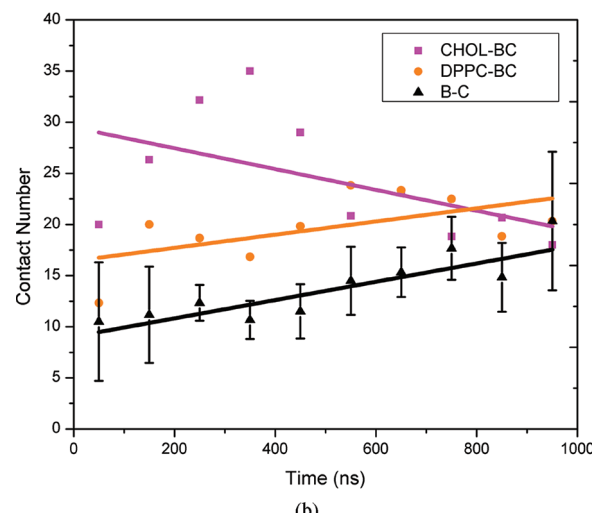
Figure 10. RDFs between protein and DPPC carbonyl oxygen, DPPC phosphate oxygen, DPPC nitrogen, cholesterol oxygen, and cholesterol hydrogen of the upper leaflet.

reason for the decrease of the peak height of CHO–DPPC RDF in the upper leaflet. From the RDFs, we observed that the oxygen atom on the cholesterol has a higher tendency to bind with the carbonyl groups than the phosphate groups of the DPPC. This implies that the cholesterol is predisposed to locate below the DPPC headgroup and agrees well with the study of Chiu et al.⁵⁵

To examine the hydrogen bonding affinity of the peptides with DPPC and cholesterol, we have also calculated the RDFs of the DPPC carbonyl oxygen group, DPPC phosphate oxygen group, DPPC nitrogen group, cholesterol oxygen group, and cholesterol hydroxyl hydrogen with respect to the peptides. The peaks around 1.9 Å in Figure 10 indicate that the peptides prefer to form more hydrogen bonds with cholesterol than with the DPPC. The cholesterol acts as both a hydrogen bond donor and acceptor. The lengths of hydrogen bonds are around 1.9, 2.5, and 3.5 Å. The protein shares the same characteristic as the cholesterol in having a greater tendency to form hydrogen bonds with the carbonyl oxygen group than the phosphate group at around 1.9 Å. No



(a)



(b)

Figure 11. Average contact numbers for the pairs within 3.5 nm during the time evolution between DPPC and cholesterol with peptide AB and peptide BC, respectively. Error bars indicate standard deviations of the contact number. The magenta lines are linear fits to the data set for contacts formed between cholesterol and peptide AB, and peptide BC; the orange line is for contacts formed between DPPC and peptides AB, and peptide BC. The black lines give the contacts between peptide A and peptide B and between peptide B and peptide C.

hydrogen bond is observed to form between protein and the DPPC nitrogen group in our study.

Correlation between Peptide Aggregation and Peptide–Lipid Interaction. The relationship between peptide aggregation and peptide–lipid interaction is complicated. We try to provide a quantitative description based on the metrics of contact numbers. The number of pairs within 0.35 nm between peptides, between peptides and lipids, and between peptides and cholesterol was monitored and displayed in Figure 11. The interaction between cholesterol and peptides A and B shows a negative correlation in comparison to the interaction between the two peptides (correlation coefficient is around –0.23). The interaction of DPPC with peptides A and B shows a very weak correlation with respect to the interaction between the two peptides according to our contacts number analysis (correlation coefficient is around –0.08). The same negative correlation trend is also observed between cholesterol and chain B and C (correlation coefficient is

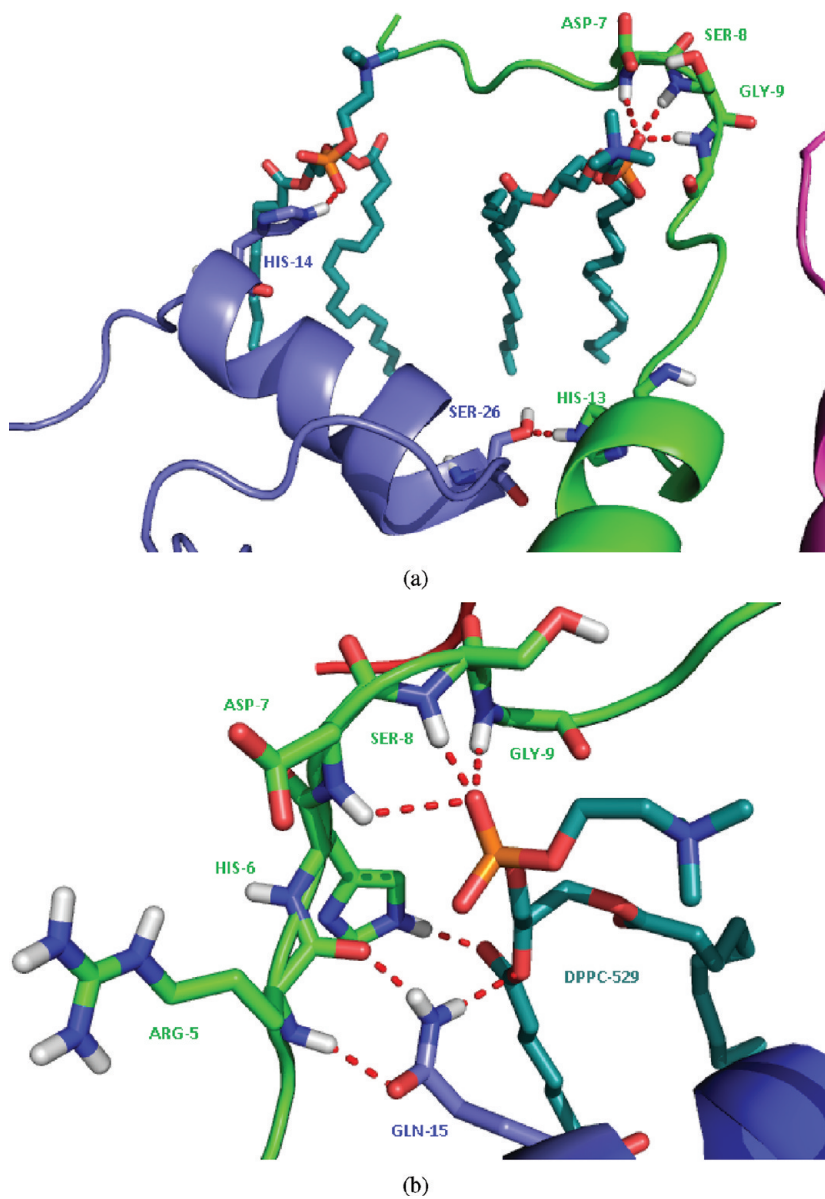


Figure 12. Snapshot of DPPC inhibiting peptide A and B aggregation at 500 ns (a). Snapshot of DPPC enhancing peptide A and B aggregation at 1000 ns (b). The residues HIS-14, GLN-15, and SER-26 from peptide A are shown as sticks and colored by elements (C, marine; N, blue; H, gray; O, red). The residues ARG-5, HIS-6, ASP-7, SER-8, GLY-9, and HIS-13 from peptide B are shown as sticks and colored by elements (C, green; N, blue; H, gray; O, red). The DPPC is also shown as sticks and colored by elements (C, cyan; N, blue; O, red; P, orange).

around -0.28), while for DPPC with peptide B and C, the correlation coefficient is around 0.34. The difference in the correlation coefficient between DPPC with peptide A and B, and DPPC with B and C, reflects the complicated relationship between peptide aggregation and peptide–lipid interactions.

The above analysis indicates that cholesterol molecules compete with peptide–peptide interaction by binding directly with peptides. This implies that monomeric $\text{A}\beta$ and/or small $\text{A}\beta$ aggregations prefer to locate within cholesterol-rich membranes.^{32,56} The binding of lipids with peptides, however, weakly enhances the already-formed aggregation of the peptides. Here through available snapshots we demonstrate some examples of lipid molecules forming hydrogen bonds with two peptide chains (see Figure 12). One example shows that DPPC inhibits peptide A and B aggregation (see Figure 12(a)). Another

example shows that the phosphate oxygen of DPPC-529 is in close proximity to the backbone amide group of residues ASP-7 (2.8 Å), SER-8 (1.8 Å), and GLY-9 (2.1 Å) from peptide B (see Figure 12(b)), which weakly enhances the already-formed aggregation of the peptides. The side chain amide group of GLN-15 from peptide A and the side chain amide group of HIS-6 from peptide B both contribute protons bonded to the nonester and ester carbonyl oxygens of DPPC-529, respectively. Here the DPPC may enhance the interaction between peptide A and B.

SUMMARY AND DISCUSSION

It is generally believed that the $\text{A}\beta$ oligomers are neurotoxic and one of the main causative factors in Alzheimer's disease. By

studying the aggregation process in mixed bilayers, we show the complicated interaction network among peptides, lipid molecules, and cholesterol. The N-terminal part of the peptide prefers to locate at the lipid–aqueous interface, while the C-terminal part inclines to bury more deeply inside the hydrophobic tails region of the lipid. A short segment of parallel β -strand is found to form between peptides B and C, and another antiparallel β -strand is observed at the C-terminal of peptide A. Meanwhile, the short sequence from 14 to 23 is found to maintain a well-preserved α -helical structure. This indicates that the force field GROMOS96, which we have used, gives a balanced description of the peptide backbone configuration. This is consistent with the recent finding of Nguyen and collaborators.⁵⁷ All these structural transitions indicate that our 1000 ns simulation has caught a glimpse of the mysterious peptide aggregation process together with the peptide secondary structure conversion from α helices to β strand.

In the mixed bilayer environment, the peptides were found to attach to the sunken membrane surface and form a hydrophilic well at the end of the simulation. The presence of the peptides has resulted in the appearance of defects in the membrane and a disordering of the cholesterol molecules. The binding of the lipids with the peptides may enhance the already-formed hydrogen bonds between peptide residues in accordance with our previous replica exchange simulation study.⁵⁸ The cholesterol molecules interact with the peptides in a competitive way resulting in a negative correlation between cholesterol–peptide interaction and peptide–peptide interaction.

We found that GLN-15 of the peptide shows a considerable importance in the aggregation process. Furthermore, ALA-42 at the C-terminus is also observed to play a noticeable role during the oligomerization in the membrane environment. We observed that the sequence HQKLVFFAED maintains a well-preserved α -helical structure in the membrane environment in the final 920 ns. Due to limited simulation time, the few small numbers of peptides used, and the lack of enhanced sampling techniques,²⁶ the complete picture of conformational transition and amyloid formation is still far beyond the reach of the current study. The aggregation of the full-length A β peptides depends on several factors such as pH, ionic strength, etc. The full understanding of the underlying mechanism still requires the joined efforts from both experimental and theoretical studies.

AUTHOR INFORMATION

Corresponding Author

*E-mail: lockyue@ntu.edu.sg; ygmu@ntu.edu.sg.

ACKNOWLEDGMENT

The authors would like to thank Hon Wai Leong from the High Performance Computing Center for his help in the provision of computational support. The authors would also like to express their appreciation to Professor Kerson Huang, Dr. Xiao Hui Qu, Dr. Xing Lin, and Ping Jiang for helpful discussions. The authors would like to thank the unknown reviewers, whose comments have substantially improved the quality of this paper. The support of the French-Singapore MERLION Programme 2009 and the College of Science collaboration grant 2011-2012 NTU is gratefully acknowledged.

REFERENCES

- (1) Evin, G.; Weidemann, A. *Peptides* **2002**, *23*, 1285–97.
- (2) Hardy, J.; Selkoe, D. J. *Science* **2002**, *297*, 353–6.
- (3) Kirkpatridge, M. D.; Bitan, G.; Teplow, D. B. *J. Neurosci. Res.* **2002**, *69*, 567–577.
- (4) Bucciantini, M.; Giannoni, E.; Chiti, F.; Baroni, F.; Formigli, L.; Zurdo, J.; Taddei, N.; Ramponi, G.; Dobson, C. M.; Stefani, M. *Nature* **2002**, *416*, 507–511.
- (5) Walsh, D. M.; Klyubin, I.; Fadeeva, J. V.; Cullen, W. K.; Anwyl, R.; Wolfe, M. S.; Rowan, M. J.; Selkoe, D. J. *Nature* **2002**, *416*, 535–539.
- (6) Resende, R.; Ferreiro, E.; Pereira, C.; de Oliveira, C. R. *Neuroscience* **2008**, *155*, 725–737.
- (7) Haass, C.; Selkoe, D. J. *Nat. Rev. Mol. Cell Biol.* **2007**, *8*, 101–112.
- (8) Kagan, B. L. *Science* **2005**, *307*, 42–43.
- (9) Wang, Q.; Walsh, D. M.; Rowan, M. J.; Selkoe, D. J.; Anwyl, R. *J. Neurosci.* **2004**, *24*, 3370–8.
- (10) Jang, H.; Zheng, J.; Lal, R.; Nussinov, R. *Trends Biochem. Sci.* **2008**, *33*, 91–100.
- (11) Jang, H.; Arce, F. T.; Ramachandran, S.; Capone, R.; Lal, R.; Nussinov, R. *J. Phys. Chem. B* **2010**, *114*, 9445–9451.
- (12) Jang, H.; Arce, F. T.; Ramachandran, S.; Capone, R.; Azimova, R.; Kagan, B. L.; Nussinov, R.; Lal, R. *Proc. Natl. Acad. Sci. U.S.A.* **2010**, *107*, 6538–6543.
- (13) Jang, H.; Arce, F. T.; Ramachandran, S.; Capone, R.; Lal, R.; low asterisk; Nussinov, R. *J. Mol. Biol.* **2010**, *404*, 917–934.
- (14) Shafir, Y.; Durell, S.; Arispe, N.; Guy, H. R. *Proteins: Struct., Funct., Bioinf.* **2010**, *78*, 3473–3487.
- (15) Sepulveda, F. J.; Parodi, J.; Peoples, R. W.; Opazo, C.; Aguayo, L. G. *PLoS One* **2010**, *5*, e11820.
- (16) Strodel, B.; Lee, J. W. L.; Whittleston, C. S.; Wales, D. J. *J. Am. Chem. Soc.* **2010**, *132*, 13300–13312.
- (17) Xu, Y.; Shen, J.; Luo, X.; Zhu, W.; Chen, K.; Ma, J.; Jiang, H. *Proc. Natl. Acad. Sci. U.S.A.* **2005**, *102*, 5403–5407.
- (18) Lemkul, J. A.; Bevan, D. R. *Arch. Biochem. Biophys.* **2008**, *470*, 54–63.
- (19) Chang, Z.; Luo, Y.; Zhang, Y.; Wei, G. *J. Phys. Chem. B* **2011**, *115*, 1165–1174.
- (20) Jang, S.; Shin, S. *J. Phys. Chem. B* **2006**, *110*, 1955–1958.
- (21) Urbanc, B.; Cruz, L.; Ding, F.; Sammond, D.; Khare, S.; Buldyrev, S. V.; Stanley, H. E.; Dokholyan, N. V. *Biophys. J.* **2004**, *87*, 2310–2321.
- (22) Melquiond, A.; Dong, X.; Mousseau, N.; Derreumaux, P. *Curr. Alzheimer Res.* **2008**, *5*, 244–250.
- (23) Bellesia, G.; Shea, J.-E. *J. Chem. Phys.* **2009**, *131*, 111102.
- (24) Urbanc, B.; Betnel, M.; Cruz, L.; Bitan, G.; Teplow, D. B. *J. Am. Chem. Soc.* **2010**, *132*, 4266–4280.
- (25) Mitternacht, S.; Staneva, I.; Hard, T.; Irback, A. *J. Mol. Biol.* **2011**, *410*, 357–367.
- (26) Davis, C. H.; Berkowitz, M. L. *J. Phys. Chem. B* **2009**, *113*, 14480–14486.
- (27) Nikolic, A.; Baud, S.; Rauscher, S.; Pomes, R. *Proteins: Struct., Funct., Bioinf.* **2011**, *79*, 1–22.
- (28) Wang, Q.; Zhao, C.; Zhao, J.; Wang, J.; Yang, J.-C.; Yu, X.; Zheng, J. *Langmuir* **2010**, *26*, 3308–3316. PMID: 19928820
- (29) Kumar, A.; Bullard, R. L.; Patel, P.; Paslay, L. C.; Singh, D.; Bienkiewicz, E. A.; Morgan, S. E.; Rangachari, V. *PLoS One* **2011**, *6*, e18759.
- (30) Ashley, R. H.; Harroun, T. A.; Hauss, T.; Breen, K. C.; Bradshaw, J. P. *BMC Struct. Biol.* **2006**, *6*, 21.
- (31) Kakio, A.; Yano, Y.; Takai, D.; Kuroda, Y.; Matsumoto, O.; Kozutsumi, Y.; Matsuzaki, K. *J. Pept. Sci.* **2004**, *10*, 612–21.
- (32) Leoni, V.; Solomon, A.; Kivipelto, M. *Biochem. Soc. Trans.* **2010**, *38*, 1021–5.
- (33) Soscia, S. J.; Kirby, J. E.; Washicosky, K. J.; Tucker, S. M.; Ingelsson, M.; Hyman, B.; Burton, M. A.; Goldstein, L. E.; Duong, S.; Tanzi, R. E.; Moir, R. D. *PLoS One* **2010**, *5*, e9505.
- (34) Ionov, M.; Klajnert, B.; Gardikis, K.; Hatziantoniou, S.; Palecz, B.; Salakhutdinov, B.; Cladera, J.; Zamaraeva, M.; Demetzos, C.; Bryszewska, M. *J. Therm. Anal. Calorim.* **2010**, *99*, 741–747.
- (35) Kakio, A.; Nishimoto, S.-i.; Yanagisawa, K.; Kozutsumi, Y.; Matsuzaki, K. *Biochemistry* **2002**, *41*, 7385–7390.

- (36) Okada, T.; Wakabayashi, M.; Ikeda, K.; Matsuzaki, K. *J. Mol. Biol.* **2007**, *371*, 481–489.
- (37) Crescenzi, O.; Tomaselli, S.; Guerrini, R.; Salvatori, S.; D’Ursi, A. M.; Temussi, P. A.; Picone, D. *Eur. J. Biochem.* **2002**, *269*, 5642–5648.
- (38) Chiu, S.; Pandit, S.; Scott, H. L.; Jakobsson, E. *J. Phys. Chem. B* **2009**, *113*, 2748–2763.
- (39) Pandit, S. A.; Chiu, S.-W.; Jakobsson, E.; Grama, A.; Scott, H. L. *Langmuir* **2008**, *24*, 6858–6865.
- (40) Pandit, S. A.; Chiu, S.-W.; Jakobsson, E.; Grama, A.; Scott, H. L. *Biophys. J.* **2007**, *92*, 920–927.
- (41) Pandit, S. A.; Vasudevan, S.; Chiu, S. W.; Jakobsson, E.; Scott, H. L. *Biophys. J.* **2004**, *87*, 1092–1100.
- (42) Chiu, S. W.; Vasudevan, S.; Jakobsson, E.; Mashl, R. J.; Scott, H. L. *Biophys. J.* **2003**, *85*, 3624–3635.
- (43) Norton, W. T.; Abe, T.; Poduslo, S. E.; Devries, G. H. *J. Neurosci. Res.* **1975**, *1*, 57–75.
- (44) Hess, B.; Bekker, H.; Berendsen, H. J. C.; Fraaije, J. G. E. M. *J. Comput. Chem.* **1997**, *113*, 1463–1472.
- (45) Nosé, S. *Mol. Phys.* **1984**, *55*, 255–268.
- (46) Hoover, W. G. *Phys. Rev. A* **1985**, *31*, 1695–1697.
- (47) Nagle, J. F.; Tristram-Nagle, S. *Curr. Opin. Struct. Biol.* **2000**, *10*, 474–480.
- (48) Essmann, U.; Perera, L.; Berkowitz, M. L.; Darden, T.; Lee, H.; Pedersen, L. G. *J. Chem. Phys.* **1995**, *103*, 8577–8593.
- (49) DeLano, W. L. *The PyMOL Molecular Graphics System*, version 1.4; Schrödinger, LLC.: New York, 2011.
- (50) Humphrey, W.; Dalke, A.; Schulten, K. *J. Mol. Graphics* **1996**, *14*, 33–38.
- (51) Anna, S.; Joachim, S. *Biochemistry* **1974**, *13*, 4839–4845.
- (52) Kabsch, W.; Sander, C. *Biopolymers* **1983**, *22*, 2577–637.
- (53) Petkova, A. T.; Ishii, Y.; Balbach, J. J.; Antzutkin, O. N.; Leapman, R. D.; Delaglio, F.; Tycko, R. *Proc. Natl. Acad. Sci. U.S.A.* **2002**, *99*, 16742–16747.
- (54) Plumley, J. A.; Dannenberg, J. J. *J. Am. Chem. Soc.* **2010**, *132*, 1758–1759.
- (55) Chiu, S. W.; Jakobsson, E.; Mashi, R. J.; Scott, H. L. *Biophys. J.* **2002**, *83*, 1842–1853.
- (56) Friedrich, R. P.; Tepper, K.; Rönicke, R.; Soom, M.; Westermann, M.; Reymann, K.; Kaether, C.; Fändrich, M. *Proc. Natl. Acad. Sci. U.S.A.* **2010**, *107*, 1942–1947.
- (57) Nguyen, P. H.; Li, M. S.; Derreumaux, P. *Phys. Chem. Chem. Phys.* **2011**, *13*, 9778–9788.
- (58) Jiang, P.; Xu, W. X.; Mu, Y. G. *PLoS Comput. Biol.* **2009**, *5*, e1000357.